Theoretical Study of Alkali Metal Pyrrolides in Comparison with *n*H−Pyrrole

Ken R. F. Somers, Eugene S. Kryachko,* and Arnout Ceulemans

Department of Chemistry, University of Leuven, Celestijnenlaan 200 F, B-3001 Leuven, Belgium

Received: November 7, 2002; In Final Form: May 1, 2003

The purpose of the present work is to demonstrate the remarkable difference between Li-pyrrolide, on one hand, and Na and K ones, on the other, viz., if the former exists as two conformers, σ and π with a significant preference to the π, at least in the gas phase, Na- and K-pyrrolides only establish the stable π structure. A key factor of its higher stabilization is the formation of the $M^{+\delta}-N^{-\sigma}$ ionic pair (M = Li, Na, and K) where the alkali metal atom behaves as a cation interacting with the pyrrole ring via a typical π-cation interaction. The formation of alkali metal pyrrolides is related to the reactions of the N−H bond-breaking H abstraction and a further hydrogen "walk" along the pyrrole ring resulting in *n*H-pyrrole. Both reactions are thoroughly studied, and four novel pathways for the pyrolysis of pyrrole starting, by means of the 1,2 H migration, from pyrrolenine (2H-pyrrole) and exiting along the HCN-propyne channel, are proposed.

1. Introduction

Alkali metal pyrrolides as the derivatives of pyrrole, with the hydrogen in the N−H bond being replaced by the metal atom, are widely used as reactants in a variety of chemical and biochemical reactions.[1] An early theoretical study, conducted by Schleyer and co-workers[2] within the B3LYP/6-311+G(d,p) method, establishes two stable structures of the σ and π types for the lithium pyrrolide. The latter is energetically favored by 9.9 kcal/mol over the σ which however mimics pyrrole. What are then the structures of sodium or potassium pyrrolides which have not been reported so far and are examined to a much lesser extent, although, as well-known, sodium and potassium are more important, compared to lithium, in biological systems[3,4] and can also be treated as model systems to gain a better understanding of their bonding trends in larger biological molecules? Are they similar to the lithium pyrrolide; that is, are they also characterized by two conformers or not? If there exist two conformers of such pyrrolides, how are they then formed and what are the energetical and structural features of their bonding, in particular, how large is the activation barrier separating them from each other? Finally, what is the origin of the larger stability of the π complex despite the fact that the metal atom actually replaces the hydrogen in the N−H group? These questions will be fully addressed in the present work aimed to study the potential energy surfaces (PESs) of the interaction of Li, Na, and K with the pyrrolyl radical via ab initio quantum chemical methods. In addition, the role of the N−H bond breaking and a farther "walk" of the hydrogen atom over the ring, leading to the novel pathways in the pyrolysis of pyrrole, will be also thoroughly discussed.

2. Computational Framework and Reference Molecules

All computations, framing the present work, were performed with the hybrid density functional B3LYP potential and the second-order Møller−Plesset perturbation method (MP2) within a frozen-core approximation in conjunction with a 6-31+G(d) (≡A) basis sets using the Gaussian 98 package of quantum chemical programs.[5] Such computational levels appear to be adequate for the reported geometry optimizations. However, they were further refined at the MP2/6-311++G(2d,2p) (≡B) level, also with a frozen core. The harmonic vibrational frequencies and corresponding zero-point vibrational energies (ZPVE) were calculated at all employed computational levels in order to distinguish whether these structures belong to the local energy minima or to saddle points and to obtain the thermodynamic quantities such as enthalpy and entropy. The basis set superposition error (BSSE) was accounted for by means of the known counterpoise procedure implemented in Gaussian 98. The expectation value of the $\mathbf{S}^2$ operator for radicals was kept equal to 0.750. Furthermore, all geometrical parameters and harmonic frequencies in the text are referred to the B3LYP/A computational method unless otherwise mentioned. The intrinsic reaction coordinate (IRC) calculations were performed for all transition structures in the novel pathways of the pyrolysis of pyrrole.

2.1. Ground-State Pyrrole Molecule and the Three Lowest States of the Pyrrolyl Radical. The ground electronic state of the pyrrole molecule (Pyr), assigned to the $^1A_1$ irreducible representation of the C_{2v} point group (Figure 1), its two lowest states of the symmetry $^1A_2$ and $^1B_1$, and the three lowest energy states of the pyrrolyl radical ($Pyr^{\bullet}$), corresponding to $^2A_2$, $^2A_1$, and $^2B_1$ within the same point symmetry are naturally chosen in the present work as the reference states of pyrrole and pyrrolyl to verify the accuracy of the B3LYP/A and MP2/A computational methods. Their optimized bond lengths and bond angles are surveyed in Tables 1 and 2 and Figure 1 and, overall, show a rather perfect agreement with the experimental[7] and early theoretical data.[6,8] As anticipated, the hydrogen abstraction of the $^1A_1$ ground-state pyrrole, yielding the ground-state pyrrolyl radical of the symmetry $^2A_2$, results in the lengthening of the C_2-C_3 and C_4-C_5 bonds by about 0.07−0.08 Å and the shortening of the others, $N-C_2$, $N-C_5$, and C_3-C_4, by 0.03 and 0.06 Å, respectively. The latter then becomes the double bond.

The geometrical changes, taking place under the hydrogen abstraction from the N−H bond of pyrrole, are naturally accompanied by those in its vibrational spectrum presented in

* To whom correspondence should be addressed. Present address: Departement SBG, Limburgs Universitaire Centrum, Universitaire Campus, B-3590 Diepenbeek, Belgium. Fax: +32 (11) 26 83 01. E-mail: eugene.kryachko@luc.ac.be. On leave from Bogoliubov Institute for Theoretical Physics, Kiev, 03143 Ukraine.

10.1021/jp022382w CCC: $25.00
Published on Web 06/20/2003

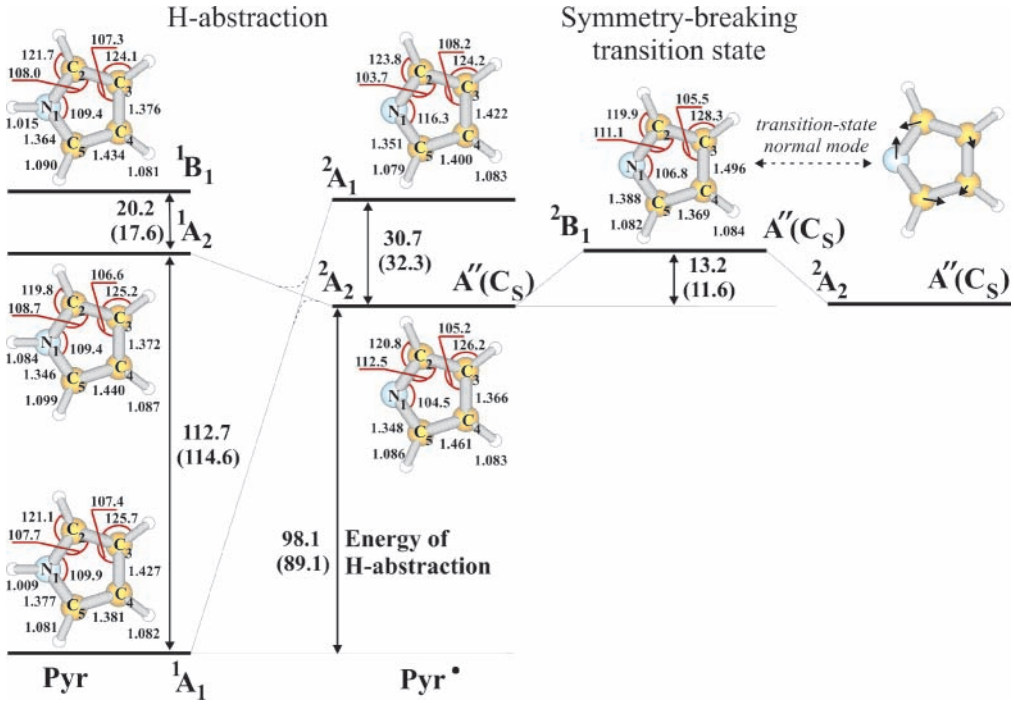

Figure 1. Three B3LYP/A lower-energy states of pyrrole and the pyrrolyl radical demonstrating the hydrogen abstraction reaction pathway via the crossing. Energies are given in kcal/mol, distances in Å, and angles in degrees. The ZPVE-corrected energies are indicated in parentheses. The clockwise enumeration of atoms in pyrrole is valid throughout the present work.

TABLE 1: C_{2v}-Optimized Geometry of the $^1A_1$ Ground Electronic State of Pyrrole (Asterisk Indicates the Present Work)[a]

geometry	B3LYP/ A*	B3LYP/ cc-pVTZ [ref 6a]	MP2/ A*	MP2/ DZP [ref 6b]	MP2/ B*	CASSCF/ cc-pVDZ [ref 6c]	expt [ref 7]
$r(N_1-C_2)$	1.377	1.371	1.375	1.375	1.372	1.367	1.370
$r(N_1-H_1)$	1.009	1.003	1.012	1.007	1.004	0.995	0.996
$r(C_2-C_3)$	1.381	1.374	1.386	1.391	1.385	1.374	1.382
$r(C_2-H_2)$	1.081	1.076	1.082	1.078	1.074	1.077	1.076
$r(C_3-C_4)$	1.427	1.421	1.421	1.424	1.420	1.452	1.424
$r(C_3-H_3)$	1.082	1.077	1.083	1.079	1.075	1.078	1.077
$\angle C_2N_1C_3$	109.9	109.8	110.2	110.3	110.2	110.0	109.8
$\angle N_1C_2C_3$	107.7	107.7	107.4	107.4	107.4	108.3	107.7
$\angle N_1C_2H_2$	121.1	121.3	121.3	121.2	121.3	121.1	121.6
$\angle C_2C_3C_4$	107.4	107.4	107.5	107.5	107.5	106.7	107.4
$\angle C_2C_3H_3$	125.7	125.7	125.6	127.2	125.5	126.1	127.1

[a] The atomic labelling is shown in Figure 1. The bond length $r(X_k-Y_l)$ is defined as the distance between the atoms X_k and Y_l in Pyr. Bond lengths are given in Å, and bond angles are in degrees.

TABLE 2: Optimized Geometries of the Three Lowest States of the Pyrrolyl Radical of the C_{2v} Symmetry $^2A_2$ (the Ground Electronic State), $^2A_1$, and $^2B_1$ (Asterisk Refers to the Present Work)[a]

	$^2A_2$				$^2B_1$	$^2A_1$
geometry	B3LYP/ A*	B3LYP/ DZP++ [ref 8]	MP2/ A*	MP2/ B*	B3LYP/ A*	B3LYP/ A*
$r(N_1-C_2)$	1.348	1.351	1.340	1.336	1.388	1.351
$r(C_2-C_3)$	1.461	1.466	1.447	1.446	1.369	1.400
$r(C_2-H_2)$	1.086	1.089	1.085	1.079	1.082	1.079
$r(C_3-C_4)$	1.366	1.370	1.378	1.376	1.496	1.422
$r(C_3-H_3)$	1.085	1.085	1.083	1.076	1.084	1.083
$\angle C_2N_1C_3$	104.5	104.6	104.2	104.5	106.8	116.3
$\angle N_1C_2C_3$	112.5	112.5	113.1	113.0	111.1	103.7
$\angle N_1C_2H_2$	120.8	120.9	120.6	120.8	119.9	123.8
$\angle C_2C_3C_4$	105.2	105.2	104.8	104.8	105.5	108.2
$\angle C_2C_3H_3$	126.2	126.3	126.7	126.7	128.3	124.2

[a] The atomic labelling is shown in Figure 1. Bond lengths are given in Å, and bond angles are in degrees.

Table 3. For example, the ν_{14} mode of pyrrole, assigned to the stretching of the N−C_2, N−C_5, and C_3−C_4 bonds, becomes blue-shifted by 31 cm^{-1} due to their contractions under the hydrogen abstraction. Table 3 gathers the most recently avalaible experimental and theoretical spectra of pyrrole and the pyrrolyl radical in their three aforementioned lowest electronic states. Notice that the modes ν_1, ν_{17}, and ν_{24} of pyrrole correspond to the out- and in-plane bending and stretching of the N−H bond.

The three lowest states of pyrrole and the pyrrolyl radical are schematically displayed in Figure 1. The present excitation energies, 114.6 and 132.2 kcal/mol taken after ZPVE, of the two lowest states of pyrrole of the symmetry $^1A_2$ and $^1B_1$ are in a fair agreement with the experimental and recent CASPT2 data (115.8 and 135.4 kcal/mol) by Roos and co-workers.[10] The lowest energy state of the pyrrolyl radical of symmetry $^2A_1$ appears to be less stable by ≈31 kcal/mol compared to the $^2A_2$ one (30.7 and 32.3 kcal/mol at B3LYP/A without and with ZPVE and 31.9 kcal/mol at MP2/B computational level). This value satisfactorily agrees with the G2(MP2) magnitude (≈34 kcal/mol) obtained by Bacskay at al.[11] As follows from Tables 1 and 2, such a state of pyrrolyl geometrically resembles the parent ground-state pyrrole molecule, which implies that the N−H bond-breaking H abstraction reaction pathway proceeds via the crossing of the A_1 and A_2 PESs (see also ref 11). The fact that the $^1A_2$ state of pyrrole correlates with the $^2A_2$ state of the pyrrolyl radical, yielding the crossing, is confirmed first by their geometrical mimicry and, second, stems out from that the length of the N−H bond of the $^1A_2$ state of pyrrole is equal to 1.084 Å, thus showing a readiness of the hydrogen atom to departure (the N−H bond breaking). It is also seen from Table 3 that the corresponding N−H stretch mode exhibits a striking red shift of 1618 cm^{-1} compared to that inherent for the ground-state pyrrole. The binding energy of the N−H bond of pyrrole is then found equal to 89.1 kcal/mol (after ZPVE at the lower B3LYP/A computational level) which demonstrates a quite good agreement with the computational data, reported by Bacskay et al.[11] and which were obtained using MP2 and QCISD(T)

TABLE 3: Vibrational Spectra of the C_{2v}-Optimized Geometries of the $^1A_1$ Ground State of Pyrrole and the Three Lowest States of the Pyrrolyl Radical of the Symmetry $^2A_2$, $^2A_1$, and $^2B_1$[a]

	pyrrole									pyrrolyl radical							
			$^1A_1$			$^1A_2$		$^1B_1$		$^2A_2$				$^2B_1$		$^2A_1$	
	B3LYP/ A*	expt [ref 9]	B3LYP/ cc-pVTZ [ref 6a]	MP2/ A*	MP2/ DZP [ref 6b]		B3LYP/ A*		B3LYP/ A*	B3LYP/ A*		B3LYP/ DZP++ [ref 8]	MP2/ A*		B3LYP/ A*		B3LYP/ A*
1 b_1	478	474	484	416	498	a_2	446	a_2	471								
2 a_2	625	618	632	557	604	b_1	474	b_1	541	a_2	490	486	480	b_1	346	a_2	622
3 b_1	636	626	644	617	619(a_2)	b_1	734	b_1	716	b_1	542	537	560	a_2	507	b_1	647
4 a_2	680	712	694	623	638 (b_1)	b_2	748	b_2	749	b_2	672	678	692 (b_1)	b_1	702	b_1	752
5 b_1	727	720	733	691	692	b_1	836	b_1	865	b_1	709	709	798 (a_2)	a_2	750	b_2	812
6 b_1	827	826	838	753	763	a_2	853	a_1	880	a_2	821	816	869 (b_1)	a_1	867	a_2	829
7 b_2	876	863	882	761 (a_2)	793	a_2	858	a_2	898	b_1	837	833	872 (a_2)	b_1	873	a_1	863
8 a_2	879	868	884	878 (b_2)	870	a_2	922	b_2	957	a_2	880	871	898	a_2	886	a_2	1011
9 a_1	989	880	903	899	890	b_2	960	a_2	959	a_2	904	898	898 (b_2)	b_2	928	a_2	1035
10 a_1	1041	1018	1035	1063	1053	b_2	985	b_1	1039	b_2	943	932	1045	a_1	944	b_2	1064
11 b_2	1074	1049	1069	1087 (a_1)	1073	a_1	1056	b_2	1052	a_1	1052	1041	1096	a_1	1077	a_1	1081
12 a_1	1099	1047	1093	1127 (b_2)	1117	a_1	1075	a_1	1071	b_2	1087	1084	1125 (a_1)	b_2	1086	a_1	1172
13 b_2	1169	1134	1158	1184 (a_1)	1179 (a_1)	a_1	1189	a_1	1083	a_1	1098	1085	1272	a_1	1143	b_1	1181
14 a_1	1175	1148	1175	1195 (b_2)	1188 (b_2)	b_2	1204	a_1	1170	a_1	1206	1196	1322 (b_2)	b_2	1295	b_2	1251
15 b_2	1318	1287	1318	1331	1324	b_2	1316	b_2	1247	b_2	1306	1285	1342	a_1	1381	a_1	1346
16 a_1	1430	1391	1418	1460	1462	b_2	1437	b_2	1323	b_2	1368	1351	1468 (a_1)	b_2	1465	b_2	1349
17 b_2	1464	1424	1450	1504	1516	a_1	1475	a_1	1467								
18 a_1	1508	1470	1502	1524	1529	a_1	1551	b_2	1474	a_1	1447	1441	1601	a_1	1489	a_1	1443
19 b_2	1585	1521	1577	1583	1582	a_1	2049	a_1	1549	a_1	1568	1555		b_2	2364i	b_2	1455
20 b_2	3250	3116	3233	3283	3316	a_1	3110	b_2	2981	b_2	3225	3208	3272	b_2	3241	b_2	3235
21 a_1	3261	3125	3244	3294	3330	b_2	3131	a_1	3103	a_1	3228	3212	3279	a_1	3249	a_1	3250
22 b_2	3278	3140	3259	3308	3345	b_2	3183	b_2	3274	b_2	3249	3238	3284	b_2	3265	b_2	3295
23 a_1	3283	3148	3265	3314	3351	a_1	3186	a_1	3292	a_1	3268	3259	3305	a_1	3273	a_1	3300
24 a_1	3667	3527	3674	3670	3754	b_1	4796	a_1	3609								

[a] Frequencies are given in cm^{-1}. The data, marked by the asterisk, refer to the present work.

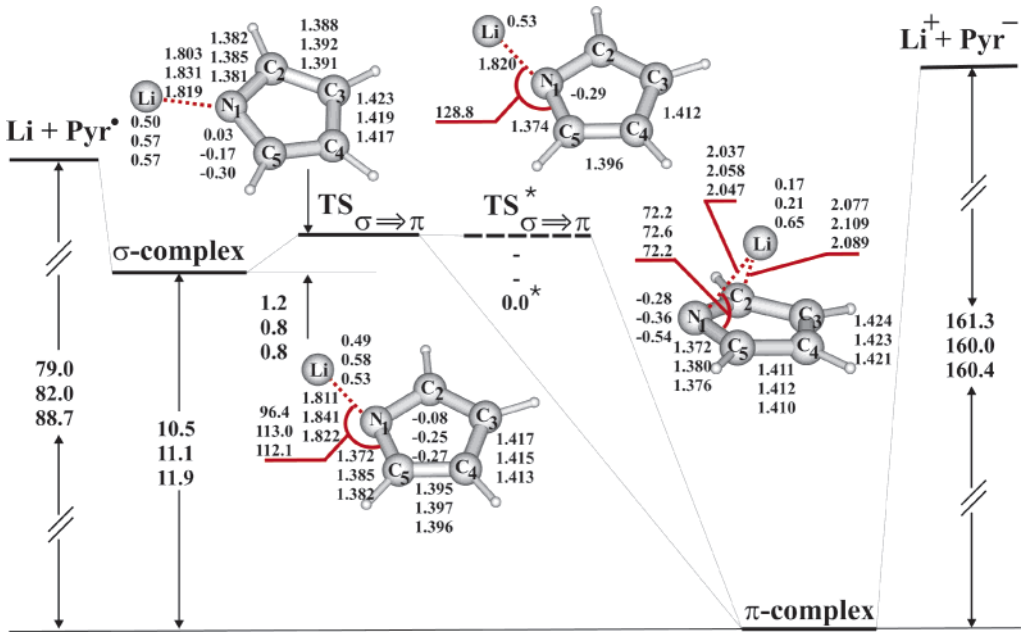

Figure 2. Li−pyrrolide complex. The bond lengths (in Å), bond angles (in degrees), and the Mulliken charges (in a.u.) on Li and N and the uncorrected relative energies (for the ZPVE and BSSE corrections see section 3) are displayed in the following order (reading from the top down, respectively): B3LYP/A, MP2/A, and MP2/B. For notations, see the text and Table 4.

methods with larger basis sets. In the present work, we assign the lowest $^2B_1$ state of the pyrrolyl radical, placed 11.6 kcal/mol above its ground state (≈12 kcal/mol in ref 11), to the transition-state linker with the imaginary frequency of 2364i cm^{-1} (its normal vector displacements are shown in Figure 1).

3. Li-Pyrrolides

According to Schleyer and co-workers[2], Li-pyrrolide exists in two different conformers. One is the σ structure of C_{2v} symmetry, where the hydrogen atom of the N−H bond of the parent pyrrole is directly replaced by Li forming the Li−N bond with a bond length of 1.803 (B3LYP/A), 1.831 (MP2/A), and 1.819 (MP2/B) Å. The other is the π characterized by C_s symmetry, with Li being placed above the pyrrolyl ring. Figure 2 pictures the PES of the Li-pyrrolide complex calculated at all employed computational levels. As shown therein, the π structure occupies the global energetic minimum, whereas the σ is located 11.1 (MP2/A) [11.9 (MP2/B); 10.5 (B3LYP/A)]

TABLE 4: Key Features of Li-Pyrrolide[a]

structure	B3LYP/A	MP2/A	MP2/B
Li-pyrrolide			
σ			
-energy	217.12147	216.39551	216.54327
ZPVE	44.7	44.5	44.5
-enthalpy	217.04490	216.31904	216.46600
entropy	74.1	75.3	74.9
dipole	8.3	8.6	8.5
$\nu_{Li}^{bend-of-plane}$	87 (64)	64 (64)	71 (63)
$\nu_{Li}^{bend-in-plane}$	98 (63)	93 (66)	86 (62)
$\nu_{Li-N}^{stretch}$	604 (91)	588 (94)	587 (93)
π			
-energy	217.13821	216.41316	216.56218
ZPVE	45.6	45.7	45.4
-enthalpy	217.06109	216.33580	216.48434
entropy	68.4	68.8	68.5
diple	4.7	5.0	4.8
$\nu_{Li\perp ring}$	553 (74)	537 (77)	551 (77)
$TS_{\sigma\rightarrow\pi}$			
-energy	217.11949	216.39416	216.54193 216.54201*
ZPVE	44.4	44.4	44.2 44.3*
-enthlapy	217.04402	216.31863	216.46658 216.46577*
entropy	70.9	72.2	66.9 71.3*
dipole	7.1	7.8	7.6 7.4*
ν_{ts}	75 i	95 i	91i 63i*
ν_{ts}			40i

[a] Energy and enthalpy are in hartree, ZPVE is in kcal/mol, entropy is in cal/mol T, dipole moment is in D, and some selected frequencies are in cm^{-1} (their IR activities in km/mol are given in parentheses), including the imaginary frequence ν_{ts}. The actual transition state T $S^*_{\sigma\rightleftharpoons\pi}$ computed at the MP2/B level is indicate by the asterisk.

kcal/mol higher. ZPVE reduces these energy separations by 1.9 (MP2/A), 1.0 (MP2/B), and 0.9 (B3LYP/A) kcal/mol which is demonstrated in Table 4. Let us notice that the present estimates are in a fair agreement with those reported in ref 2 on the basis of the B3LYP/6-311+G(d,p) calculations. It is also worth mentioning that the π structure lies by 82.0 kcal/mol (MP2/A) [88.7 kcal/mol (MP2/B)] or 79.0 kcal/mol (B3LYP/A) below the asymptote, composed of the infinitely separated ground-state Li and the pyrrolyl radical. The ZPVE correction comprises approximately 2.8 kcal/mol for both MP2/A and B3LYP/A methods. The BSSE one is larger and amounts to 7.2 (B3LYP/A) or 4.6 (MP2/A) kcal/mol for the σ structure and 4.5 (B3LYP/A) or 0.7 (MP2/A) kcal/mol for the π. This thereby implies that, in this particular case, in comparison with the MP2 method, B3LYP significantly overestimates the BSSE correction.

As shown in Figure 2, the transition $TS_{\sigma\rightleftharpoons\pi}$ state, which governs the $\sigma\rightleftharpoons\pi$ transition, is located only by 0.8 (MP2/A and MP2/B, although at the latter level, it is the second-order saddle point and the true transition state $TS^*_{\sigma\rightleftharpoons\pi}$ is placed <0.1 kcal/mol below it, see Table 4) or 1.2 (B3LYP/A) kcal/mol above the σ, that makes the latter highly metastable or even completely unstable because of the zero-point vibrations (the corresponding difference in enthalpy is 0.3 and 0.6 kcal/mol, respectively). The estimated rate constant of the reaction $\sigma \rightleftharpoons TS_{\sigma\rightleftharpoons\pi} \rightleftharpoons \boldsymbol{\pi}$ is equal to 4.9×10^{11} s^{-1}. However, we suggest that, because of a large polarity of the σ structure (8.5 vs 4.8 D of the π at MP2/B; see Table 4), the former can be stabilized in polar solvents. It is also interesting to mention that, because of the entropy excess of the σ structure over the transition one $TS_{\sigma\rightleftharpoons\pi}$ by ca. 3 cal/mol T (Table 4), an increase of temperature raises

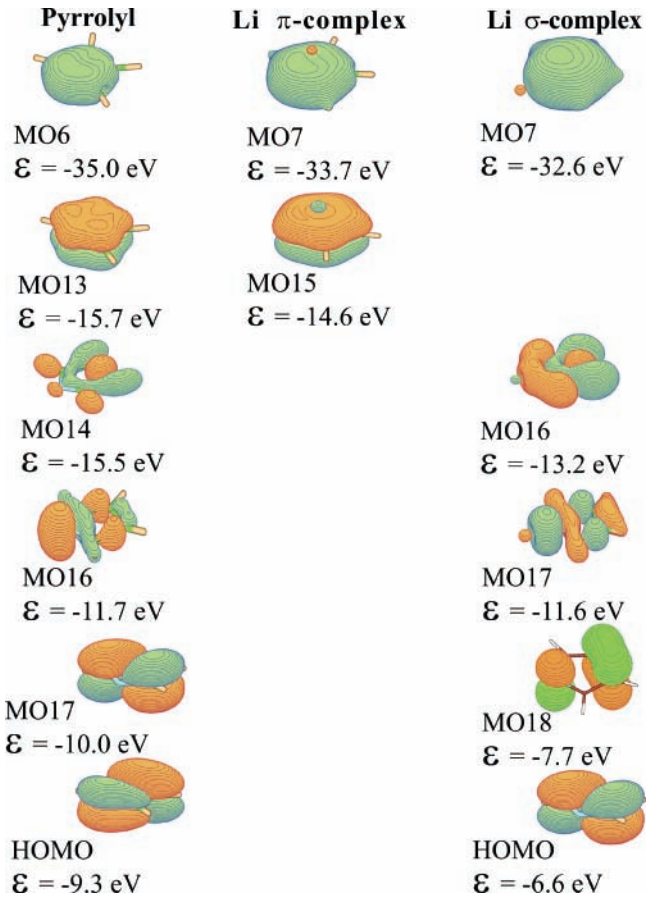

Figure 3. Some selected MP2/A MOs of the pyrrolyl radical and $\boldsymbol{\sigma}$ and $\boldsymbol{\pi}$ complexes of Li-pyrrolide. ϵ stands for the orbital energy.

the stability of the former. For example, at room-temperature T = 298.15 K, the entropy factor increases the free energy difference between σ and $TS_{\sigma\rightleftharpoons\pi}$ by 0.9 kcal/mol. On the contrary, the π structure disfavors a temperature raising.

Let us question why the π structure of Li-pyrrolide is more stable than the σ. The π structure is placed below σ by 10.5 kcal/mol (9.6 kcal/mol after ZPVE; B3LYP/A) [11.1 kcal/mol (9.9 after ZPVE; MP2/A) and 11.9 kcal/mol (10.9 after ZPVE; MP2/B)]. A key factor for a larger stabilization of the π structure is that, first, the Li and N form an ionic pair with the MP2/A Mulliken charges of 0.21 and −0.36 and a distance of 2.058 Å. A rough estimation of the ionic-pair energy gives ≈14.0 kcal/mol. Second, the formation of the $Li^{+\delta}-N^{-\sigma}$ ionic pair partly bares the Li atom so it likely behaves as a cation which, in turn, interacts with the pyrrole ring via a π-cation interaction (see ref 4d for current review), mainly with the π clouds on the carbon atoms C_2 and C_5, causing thus an elongation (by 0.02 Å) of the neighboring C−C bonds compared to that in the ground-state pyrrolyl radical. Notice that the π structure is located 161.3 kcal/mol (158.4 kcal/mol after ZPVE; B3LYP/A) or 160.0 kcal/mol (156.7 kcal/mol after ZPVE; MP2/A) and 160.4 kcal/mol (MP2/B) relative to the separated ground-state ions Li^+ and Pyr^-. As shown in Figure 2, Li is placed at the distance of ca. 2.1 Å from the neighboring carbons C_2 and C_5 in the π structure of Li-pyrrolide because of primarily the electrostatic interaction between $Li^{+\delta}$ and $N^{-\sigma}$. Such distance is smaller than that in the Li^+−benzene complex.[4d,4f] This implies that the π interaction between Li and the pyrrole ring in the π Li-pyrrolide is substantially larger.

These conclusions are supported by the molecular orbital (MO) patterns drawn in Figure 3. The lowest bonding MO in

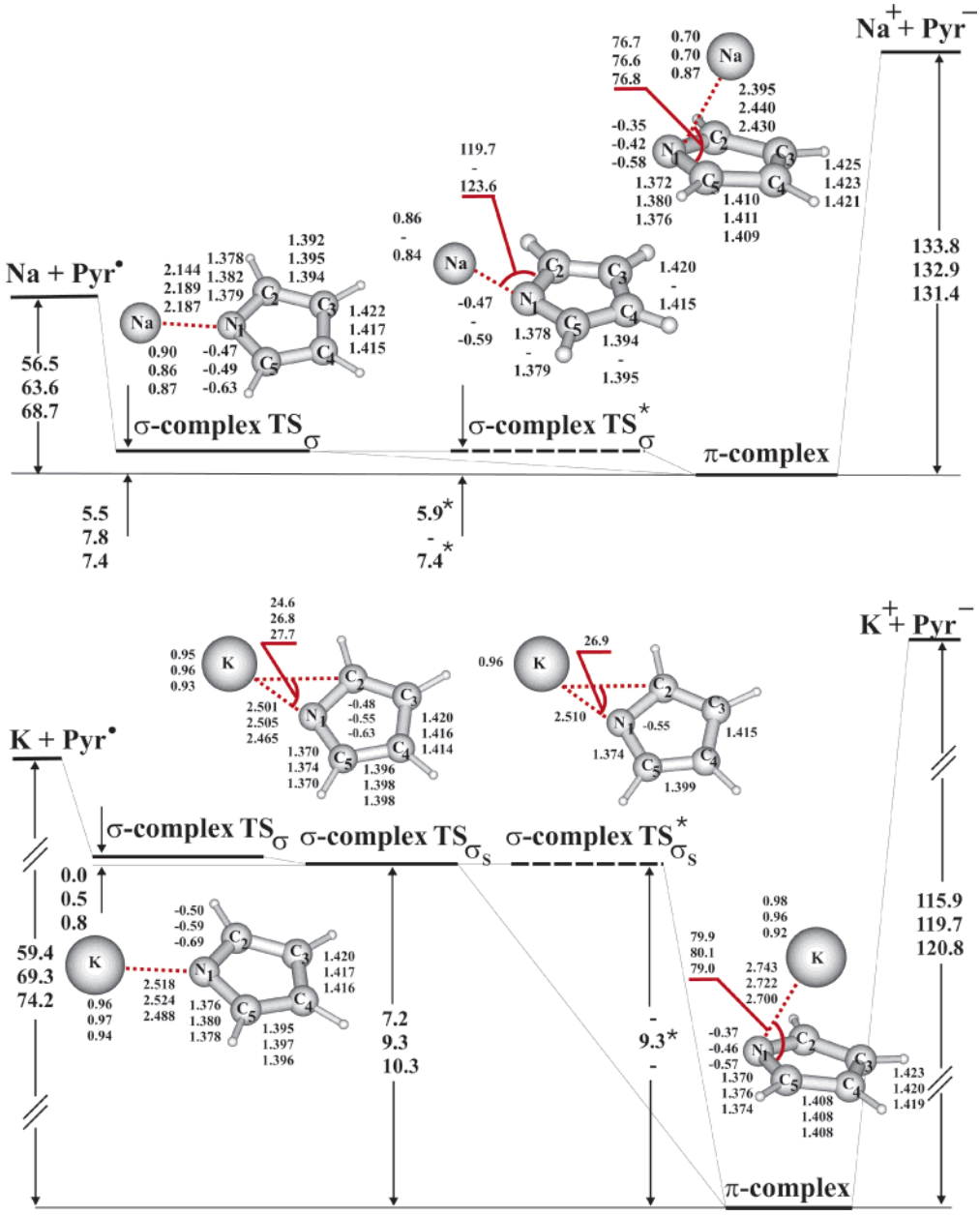

Figure 4. Na- and K-pyrrolide PESs. The B3LYP/A and MP2 values of the bond lengths in Å and bond angles in degrees are indicated by analogy with Figure 2. For notations, see the text and Tables 5 and 6.

both structures of Li-pyrrolide is MO7 corresponding to the MO6 of pyrrolyl with the orbital energy $\epsilon_{MO6} = -35.0$ eV. The analysis of the orbital occupancies of MO7 clearly demonstrates the binding character of both complexes. The apparent nodal plane is residue from the 2s MO of Li. As seen in Figure 3, the bonding between Li and pyrrolyl within MO7 is stronger for the π structure than for the σ reflecting the formation of the ionic pair in the former: first, the ϵ^{π}_{MO7} is lower by 1.1 eV compared to ϵ^{σ}_{MO7}; second, the changes of both parts of MO7 under the formation of the π Li-pyrrolides are more substantial than those in MO7 of σ whose parts are only slightly different from the pyrrolyl ones.

4. Sodium and Potassium Pyrrolides

Moving down in the periodic table, we might expect that the structures of Na- and K-pyrrolides resemble those of lithium, drawn in Figure 2, and retain their features. This is however not the case. The corresponding PESs are displayed in Figure 4 and appear slightly simpler, particularly for Na, compared to Li. This is due to the fact that, in the case of Na, the MP2/A method shows that the σ structure plays the role of the "bump"-like transition state TS_σ (the true transition state at the B3LYP/A and MP2/B levels is TS^*_σ), which bifurcates the reaction pathway with the slope of 44 cm^{-1} from the infinitely separated ground-state Na and the pyrrolyl radical $^2A_2$ to the isomeric π structures, distinct by the disposition of Na relative to the ring (above or below).

Returning to the PES of the Na-pyrrolyl radical complexation, drawn in Figure 4, we may notice that the π structure is located below the bump-like transition state TS_σ (for MP2/A) or TS^*_σ (valid for B3LYP/A and MP2/B) by 7.8 kcal/mol at MP2/A (B3LYP/A estimates it as 5.9 kcal/mol) and 7.4 kcal/mol at MP2/B (see Table 5). After taking the ZPVE correction, these values are slightly lowered to 6.9 kcal/mol (both MP2/A and MP2/B) and 5.2 kcal/mol (B3LYP/A). The sodium atom in the former structure distances from N by about 2.4 Å, forming

TABLE 5: Key Features of Na-Pyrrolide[a]

structure	B3LYP/A	MP2/A	MP2/B
Na-pyrrolide			
π			
-energy	371.89110	370.79373	370.94436
ZPVE	44.3	44.6	44.2
-enthalpy	371.81520	370.71739	370.86765
entropy	73.8	73.8	73.7
dipole	7.3	7.6	7.5
$\nu_{Na\perp ring}$	312 (42)	311 (43)	161 (6)
TS_σ			
-energy	371.88233	370.78127	370.93265
	371.88177*		370.93263*
ZPVE	44.0	43.7	43.7
	43.8*		43.7*
-enthalpy	371.80647	370.70648	370.85608
	371.80599*		370.85699*
entropy	79.0	75.2	81.8
	75.1*		75.1*
dipole	10.3	11.0	10.9
	9.8*		10.7*
ν_{ts}		44*i*	
	58*i**		28*i**

[a] Energy and enthalpy are in hartree, ZPVE is in kcal/mol, entropy is in cal/mol T, dipole moment is in D, and some selected frequencies are in cm^{-1} (their IR activities in km/mol are given in parentheses), including the imaginary frequence ν_{ts}. The actual transition state TS^*_σ computed at the B3LYP/A and MP2/B level is indicated by the asterik.

TABLE 6: Key Features of K-Pyrrolide[a]

structure	B3LYP/A	MP2/A	MP2/B
K-pyrrolide			
TS_σ			
-energy	809.49559	808.10287	808.42321
ZPVE	43.6	43.4	43.4
-enthalpy	809.42099	808.02739	808.34879
entropy	71.7	80.3	71.8
dipole	12.3	12.6	12.2
$\nu_{ts}^{(1)}$	25*i*	41*i*	51*i*
$\nu_{ts}^{(2)}$	2*i*		38*i*
TS_{σ_s}			
-energy	809.49556	808.10361	808.42451
		808.10357*	
ZPVE	43.6	43.5	43.5
		43.5*	
-enthalpy	809.42009	808.02814	808.02724
		808.02814*	
entropy	76.8	82.2	75.1
		76.0*	
dipole	11.9	12.0	11.4
		11.9*	
ν_{ts}	29*i*		20*i*
		33*i**	
π			
-energy	809.50700	808.11844	808.44088
ZPVE	44.1	44.1	44.1
-enthalpy	809.43030	808.04168	808.36432
entropy	76.0	76.3	75.6
dipole	9.3	9.4	8.9
$\nu_{K\perp ring}$	239 (37)	245 (36)	156 (4)

[a] Energy and enthalpy are in hartree, ZPVE is in kcal/mol, entropy is in cal/mol T, dipole moment is in D, and some selected frequencies are in cm^{-1} (their IR activities in km/mol are given in parentheses), including the imaginary frequence ν_{ts}. The actual transition state $TS^*_{\sigma_s}$ computed at the MP2/A level is indicated by the asterisk.

nearly the same angle (≈76.8°) with the neighboring carbon atoms, as in the Li-π complex. Such Na−N separation implies a weaker ionic pair, compared with the Li-π structure and, therefore, a weaker π-cation interaction, which is indicated by a binding energy of 56.5 kcal/mol vs 79.0 kcal/mol for the latter one (B3LYP/A) [63.6 kcal/mol vs 82.0 kcal/mol (MP2/A) and 68.7 kcal/mol vs 88.7 kcal/mol (MP2/B)]. The BSSE correction takes, correspondingly, the following values: 4.2 and 1.4 kcal/mol for the B3LYP/A and MP2/A.

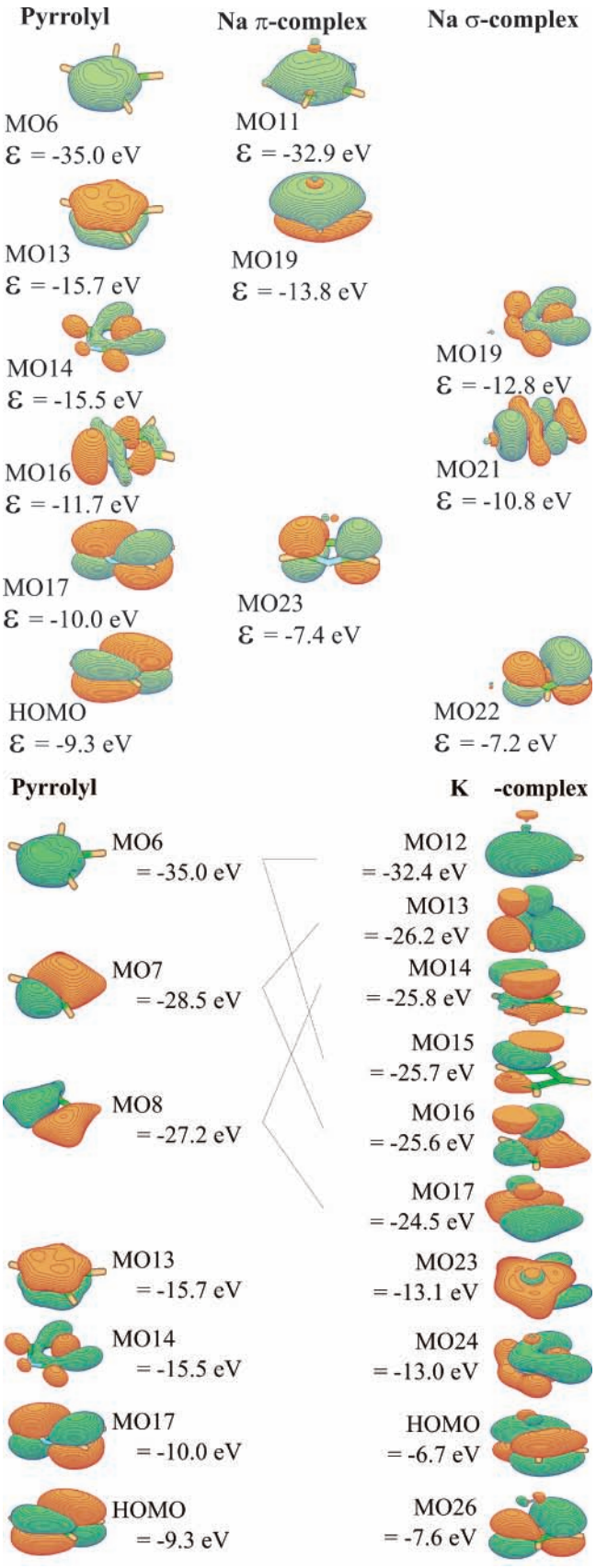

Figure 5. Shapes of some relevant MP2/A MOs of the pyrrolyl radical and σ and π complexes of Na- and K-pyrrolides. ϵ stands for the orbital energy.

The potassium atom interacts with the ground-state pyrrolyl radical in a rather different manner, which is also shown in Figure 4 (see also Table 6). A σ-type complexation of the $^2A_2$-

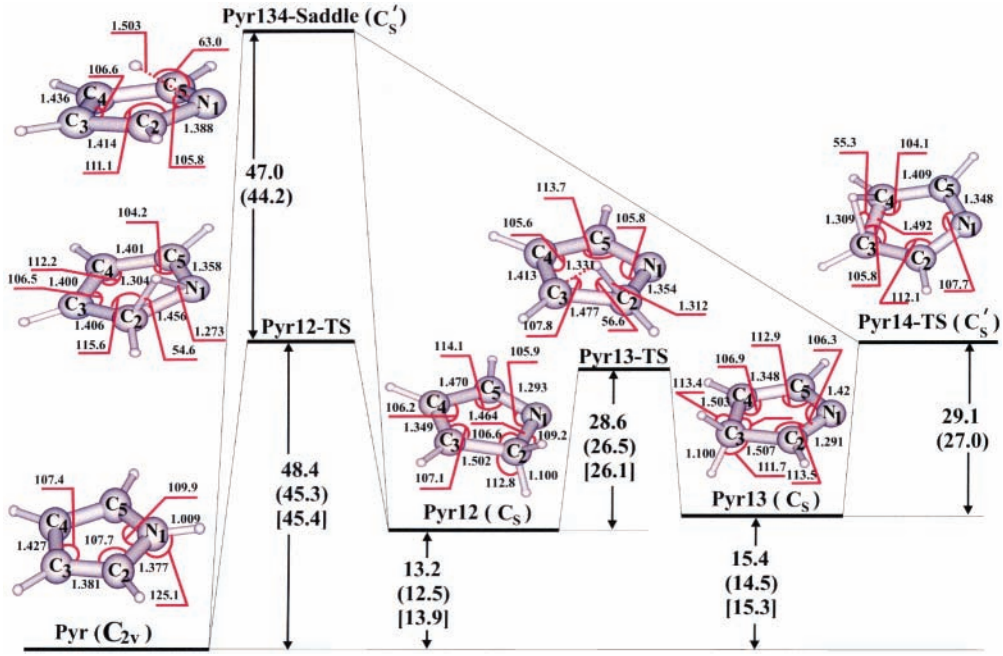

Figure 6. Hydrogen "walk" over the pyrrole ring. The B3LYP/A energies without and with the ZPVE correction (in parentheses) are given in kcal/mol, bond lengths in Å, bond angles in degrees. The G2-(MP2) energies, borrowed from ref 12e, are indicate in square brackets.[13]

CHART 1: Pathway 1

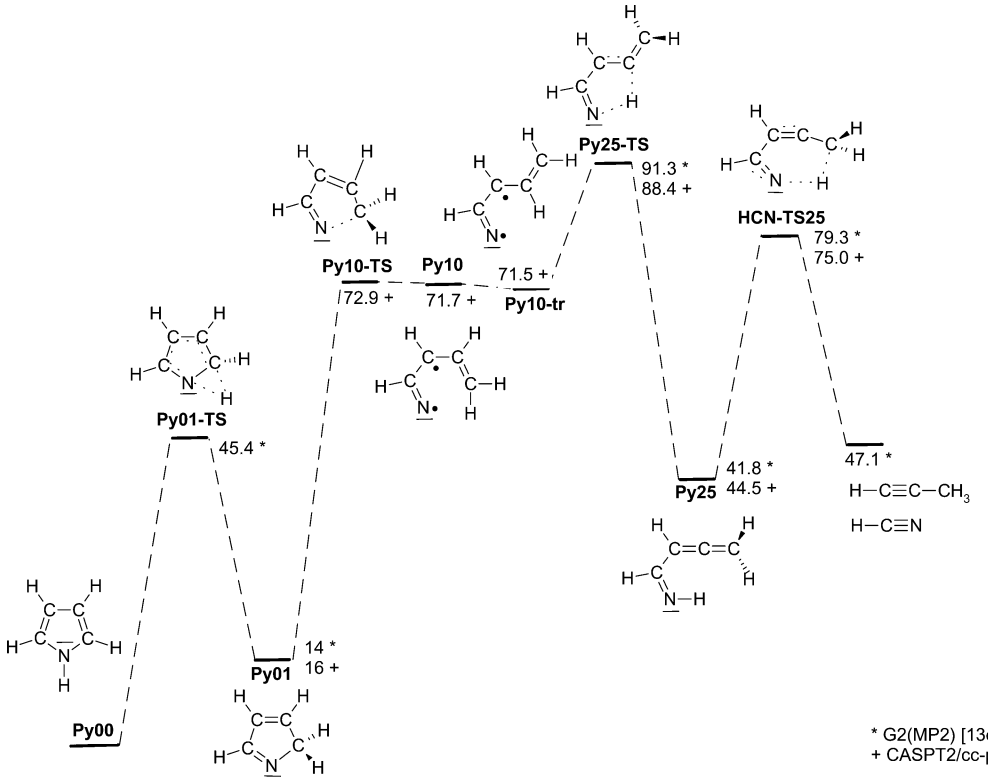

state pyrrolyl radical with K yields the second-order saddle point TS_σ on the corresponding PES (except the MP2/A level when it casts as the true transition state). Its two imaginary frequencies, being equal to 25 and 2 cm^{-1} at the B3LYP/A level and to 51 and 38 cm^{-1} at the MP2/B, govern the out- and in-plane motions of K, correspondingly, with respect to the pyrrolyl ring. The former pathway leads to the π complex whereas the latter to a novel complex TS_{σ_s} where K is placed aside the N−H bond of pyrrole forming the bonds with N and the carbon atoms C_2 and C_5. Notice that the TS_{σ_s} is slightly energetically favorable over the TS_σ: MP2/B estimates it as 0.8 kcal/mol. Interestingly, in comparison with the π Na-pyrrolide, the π K-pyrrolides lies deeper: as compared with the corresponding neutral asymptotes, the π K-pyrrolide appears to be more stable than the sodium one by 5.5 kcal/mol (MP2/B).

The shape of some relevant MO patterns of Na-pyrrolides are pictured in Figure 5. By analogy with Li-pyrrolides, the π-bonding takes place at MO6 of pyrrolyl implying thus the charge transfer and, hence, the formation of the ionic pair. It is worth mentioning that the corresponding ϵ for Na-pyrrolide is lower by 0.5 eV to that of K-pyrrolides meaning that the binding in the former is stronger. This also follows from Figure 4 where

CHART 2: Pathway 2

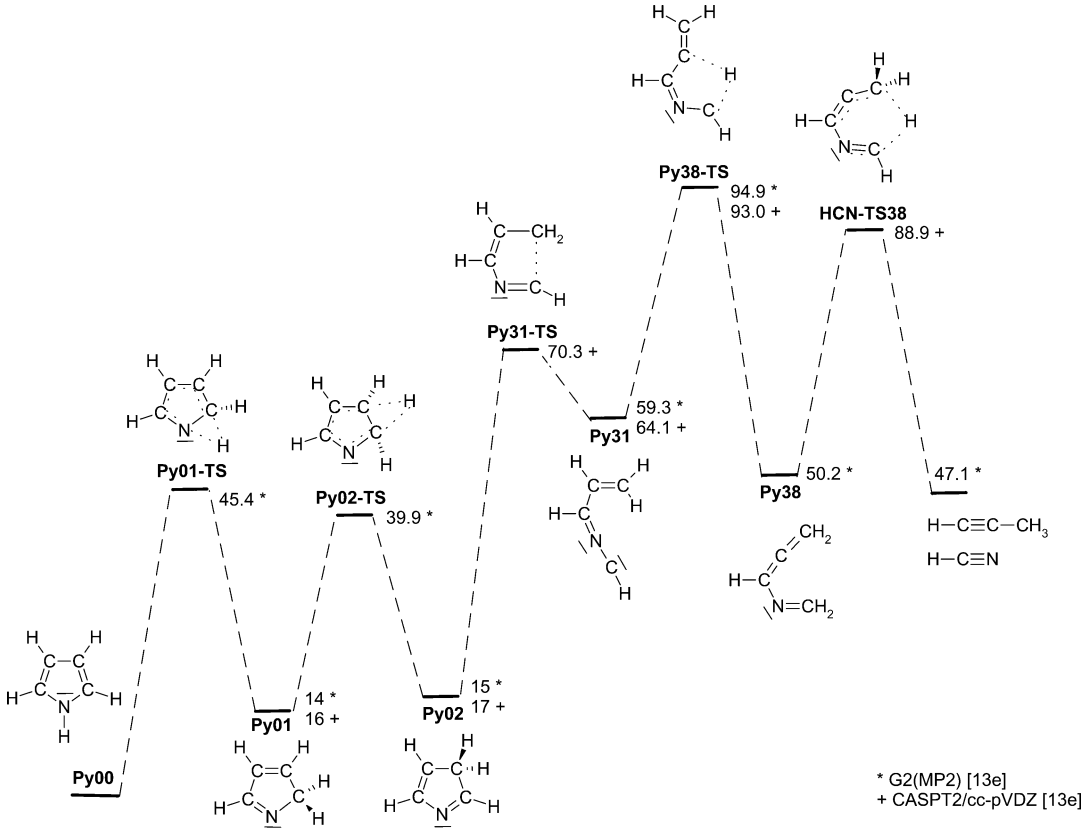

CHART 3: Pathway 3

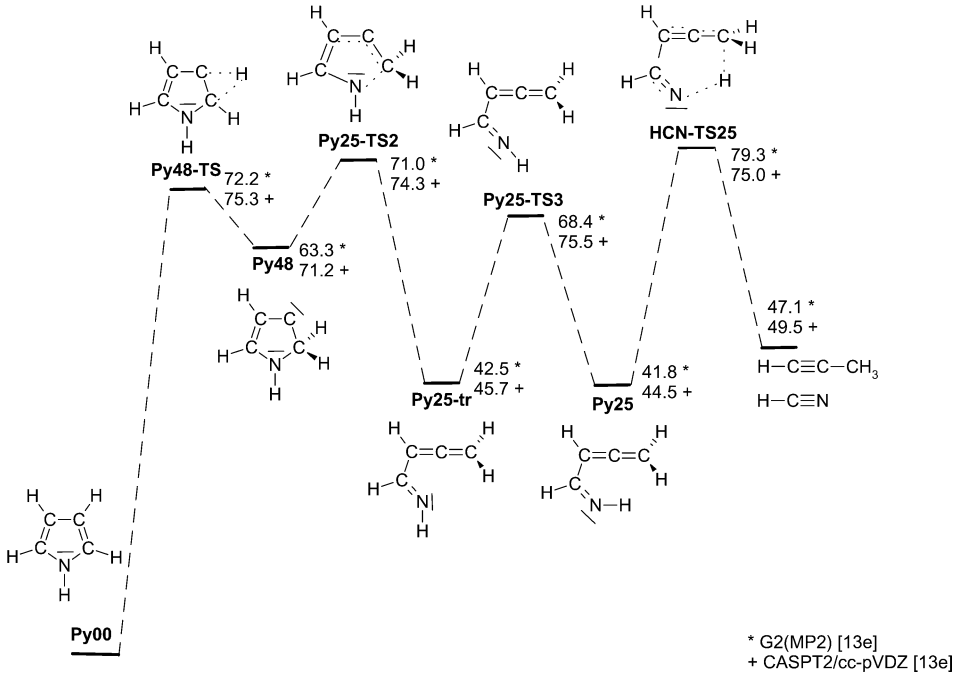

the π complex of Na-pyrrolide is placed about 10 kcal/mol lower than that of the K relative to the corresponding asymptote.

We suggest that the different behavior of the σ complexes of Li-, Na-, and K-pyrrolides is due to both the spatial extension of the interacting MOs of the metal and the bonding character of the HOMO-k with $k = 0-2$, 4, and 5 of pyrrolyl (the HOMO-3 is a nonbonding orbital because of the nodal plane passing through N and the C_2-C_3). The valence MO of Li is 2s, and it is therefore well accommodated to bind pyrrolyl, having similar molecular orbitals with a dominant covalent character that follows from Mulliken charges of 0.57 on Li and −0.17 on N. The present analysis of the MOs reveals the nonbonding character of the HOMO and the bonding character of both the HOMO-1 and the HOMO-2, the former by the π cloud and the latter by σ interactions. In contrast, the valence MO of Na is of the 3s type. A covalent interaction between Na and pyrrolyl is therefore of less importance because the overlap of the 3s with the MOs of pyrrolyl is smaller, as shown in Figure

CHART 4: Pathway 4

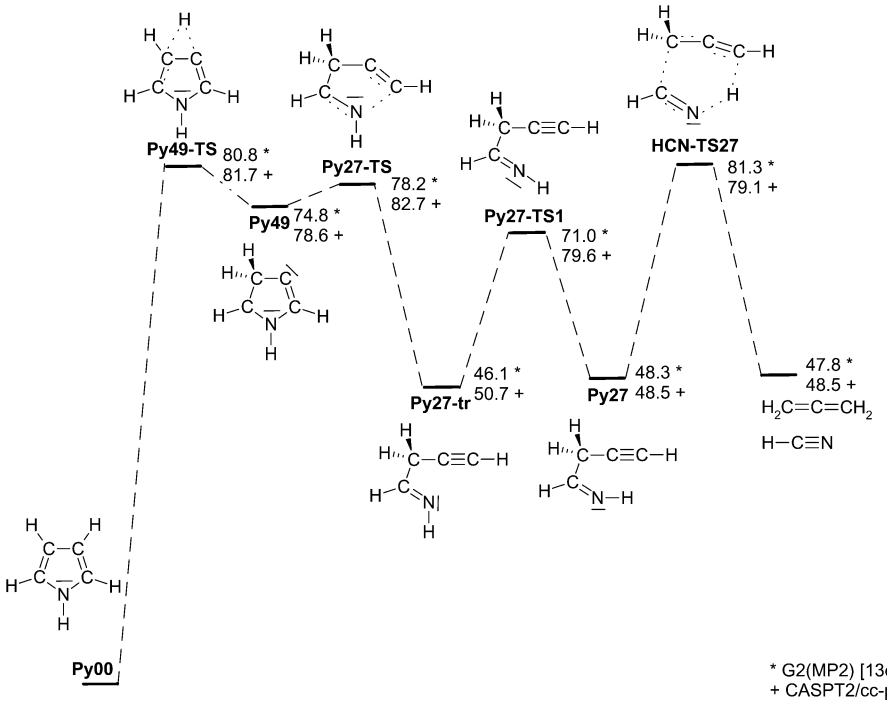

CHART 5: Pathway 5

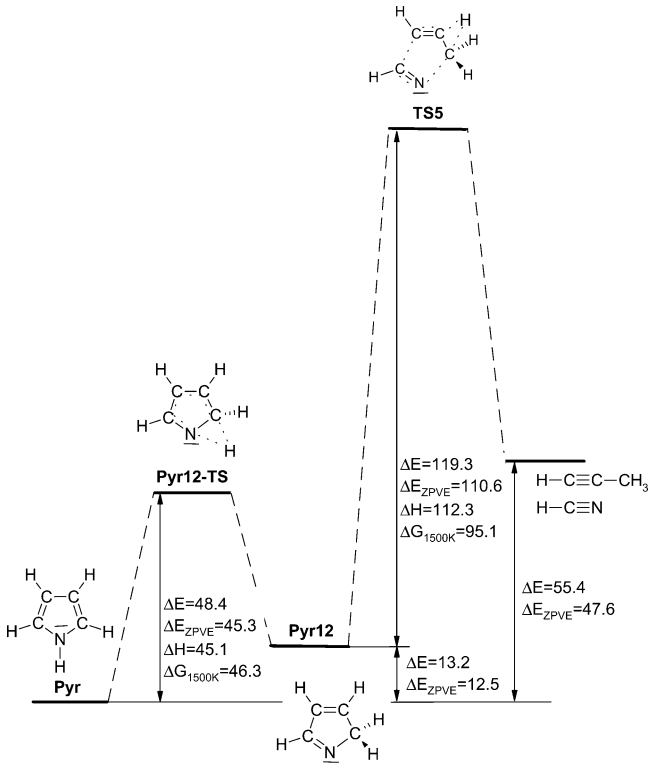

5. Such interaction is rather ionic that is confirmed by the Mulliken charges of 0.86 on Na and −0.49 on N. The stability of the σ complex with Na is lower because the HOMO-*k* (k = 0−2, 4, and 5) do not significantly contribute to the bond formation, thus leading to its high sensitivity toward out-of-plane distortions of Na. The latter increases the overlap between the Na unoccupied valence orbitals (3s and also 3p) and the π cloud of pyrollyl (see MO22 in Figure 5) promoting the formation of the π complex. The σ complex with K is described in a similar way, with the exception that the HOMO-1, which has a π character, is antibonding. It hence partly impedes the formation of the π complex opening another pathway through a saddle point. Displacements from this saddle point lead either to the π complex or to the transition state TS_{σ_s} (in-plane). The latter has nonbonding orbitals similar to those of the Na complex; however, they are more spatially extended (3*s* and 4*p*) allowing K to directly interact with both N and C_2.

5. Comparison with *n*H−Pyrrole

The present work is certainly incomplete without a thorough understanding of how the hydrogen atom of the N−H bond of pyrrole migrates over its ring, the process, which in some sense, shows us another side of the N−H breaking (cf. Figure 1). It is not only a matter of a purely academic interest aimed to compare, for example, the resultant stable *n*H-pyrrole complexes with the σ and π revealed in the present work for alkali metal pyrrolides. It also effects a matter of a significant practical value, viz., the pyrolysis of pyrrole and its major primary products such as hydrogen cyanide and propyne or allyl cyanide and crotononitrile (see refs 12 and 6c and references therein). In particular, within the model, proposed by Mackie and co-workers,[12b] the initial stage of pyrolysis of pyrrole along the HCN−propyne channel is actually its tautomerization yielding pyrrolenine or 2H-pyrrole. Such tautomerization is governed by the 1,2 H-migration transition state Pyr12-TS which, as shown in Figure 6, lies 48.4 (45.3 after ZPVE) kcal/mol above the ground electronic state of pyrrole Pyr and links it to pyrrolenine Pyr12. Such a barrier height fairly correlates with the G2-(MP2) value of 45.4 kcal/mol obtained in ref 12e (see also ref 13 for the computational note), with 44.5 kcal/mol obtained at the MP2/6−31(d) level in ref 14, and, finally, with 44.0 and 43.1 kcal/mol calculated at the B3LYP/cc-pVDZ and QCISD(T)/cc-pVDZ in ref 12d. The latter is less energetically favorable by 13.2 (12.5) kcal/mol compared to pyrrole. A farther "walk" of the hydrogen atom, initially belonging to the N−H group, along the C_2-C_3 bond results in 3H-pyrrole (Pyr13) and demands less energy (about 28.6 kcal/mol) to surmount the corresponding transition-state linker Pyr13-TS notwithstanding the fact that 3H-pyrrole is less stable than 2H-one by 2 kcal/mol. The 3,4 H-"walk" of a symmetric double-well character

CHART 6: Pathway 6

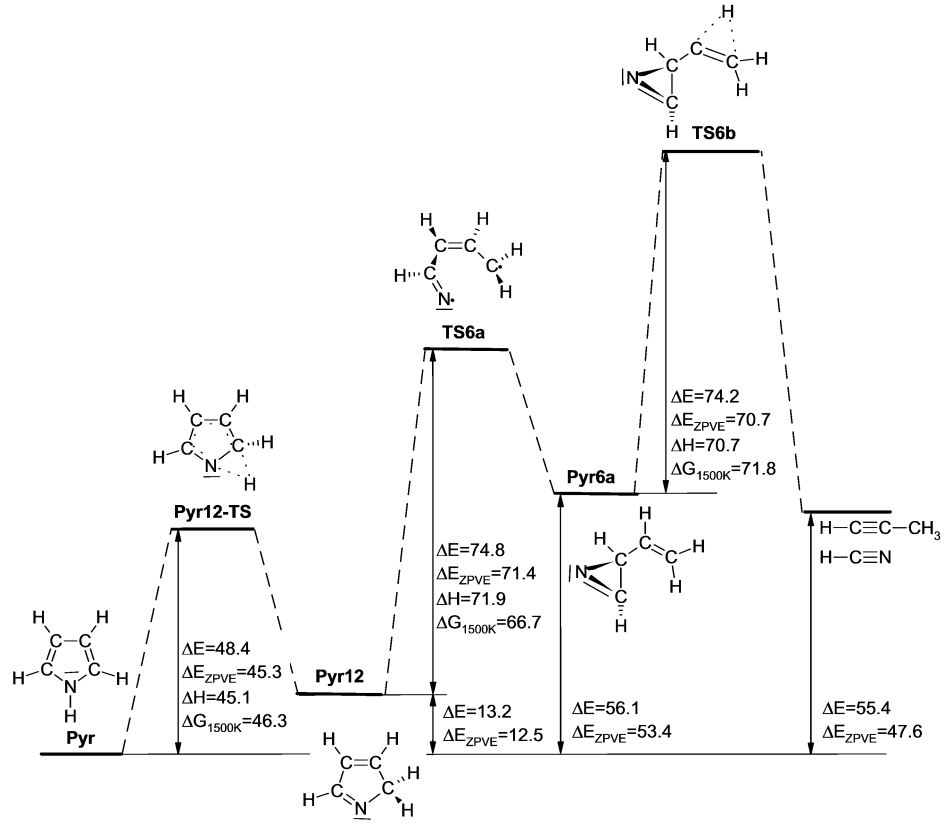

is governed by the Pyr14-TS, placed above Pyr13 by 29.1 (27.0) kcal/mol. This transition state is linked to the ground electronic state of pyrrole by the saddle structure Pyr134-Saddle of the second order which lies 95.4 (89.5) kcal/mol higher than pyrrole and actually resembles a π structure of alkali metal pyrrolides. However, in the latter case, this π structure is definitely the most stable.

The hydrogen cyanide−propyne, allyl cyanide, and crotonitrile channels of the pyrolysis of pyrrole have recently been investigated by Bacskay, Mackie, and Martoprawiro,[6c,12e] whose theoretical model of the mechanism of functioning of the former channel is based on the pathways initiated by the 1−2, 4−5, or 2−3 H migrations (in the notations of ref 12e all energies in kcal/mol are given with respect to pyrrole; Charts 1 and 2 are reconstructed from figures of ref 12e).

The portion of the PES, demonstrated in Chart 1, pictures pathway **1** and includes pyrrolenine as the first intermediate which then undergoes a ring scission and results in the open chain biradical Py10. Under the C−C bond fission, the latter yields HCN and the $CHCHCH_2$ carbene. However, as shown in ref 12e, it has to be ruled out because of its high endothermicity of about 109.5 kcal/mol at the G2-(MP2) computational level.[13] Instead, reaction **1** further proceeds to the allenic imine Py25 which concertedly decomposes into HCN and propene. The other three lower-energy pathways **2**−**4** are shown in Charts 2−4. Pathways **1**, **3**, and **4** consist of four stages, whereas **2** is characterized by five stages.

There are still other pathways started with pyrrolenine, as earlier suggested by Mackie and co-workers.[12b] They are markedly different from **1**, and we suggest that they might contribute to this channel under experimental conditions (1300−1500 K and 12 atm). These novel pathways are displayed in Charts 5−8 (all B3LYP/A energies are given in kcal/mol; see also Table 7 for energetic and thermodynamic properties of the discussed structures).

A remarkable feature and likely a certain advantage of pathway **5**, compared to **1**−**4**, is that it is actually a two-stage process. The second stage, involving the concerted break of the N−C_2 and C_4−C_5 bonds and 3,4 H-migration, is governed by the transition structure TS5 with the enthalpy difference $\Delta H = 112.3$ kcal/mol and the Gibbs free energy activation barrier $\Delta G_{1500K} = 95.1$ kcal/mol, substantially reduced because of the large entropy effect (see Table 5). Taking the ZPVE correction into account, the latter finally converts to $\Delta G_{1500K}^{ZPVE} = 86.4$ kcal/mol which is closer to the experimental activation energy of 74.1 ± 3 kcal/mol of the complete disappearance of pyrrole.[12b]

Pathway **6** consists of 3 stages and involves the formation of a nonplanar biradical transition state TS6a leading further to an azirine-based intermediate Pyr6a. The biradical transition state energy of 74.8 kcal/mol is comparable to the energy of 75.57 kcal/mol of the planar biradical transition state described in ref 12d. The resulting intermediate is characterized by its functional azirine group. Azirine is a three-membered heterocycle containing a nitrogen bound only to the cyclic carbon atoms. It is a well-known intermediate which can rearrange to form isocyanides reacting into cyanides with the activation energies of 53.0 and 67.5 kcal/mol, respectively.[15] The latter are comparable with that of TS6b that is likely another pathway to the formation of isocyanide- and cyanide-based intermediates whose presence has been shown experimentally.[12]

The remaining two pathways **7** and **8** consist of four stages evolving through a nonbiradical based ring opening TS7a which is actually a completely novel approach toward such a phenomenon. We suggest that this transition state TS7a, characterized by the activation energy of 79.3 kcal/mol, provides an interesting alternative to the biradical transition state with the energy of 57 kcal/mol earlier described in ref 12. TS7a is a planar structure with a single hydrogen placed nearly perpendicular to the plane. Its C−N bond length is 1.220 Å which is

CHART 7: Pathway 7

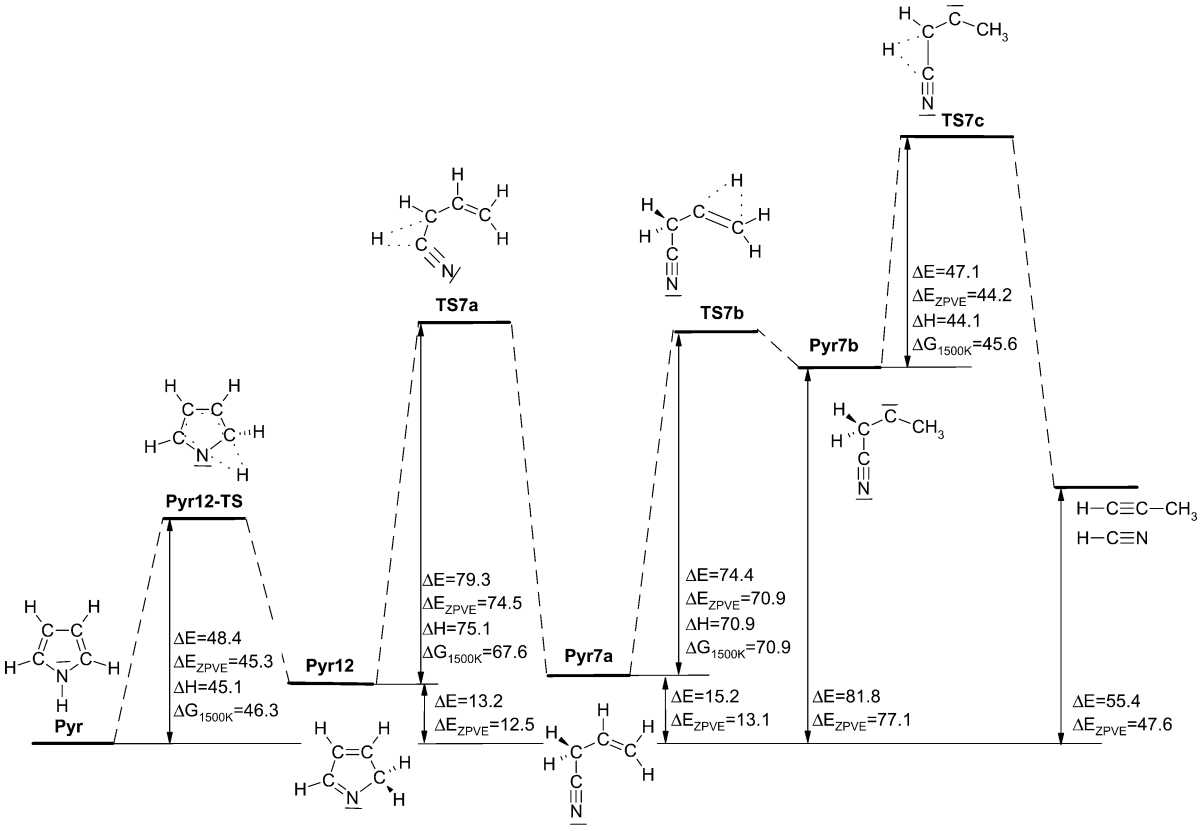

CHART 8: Pathway 8

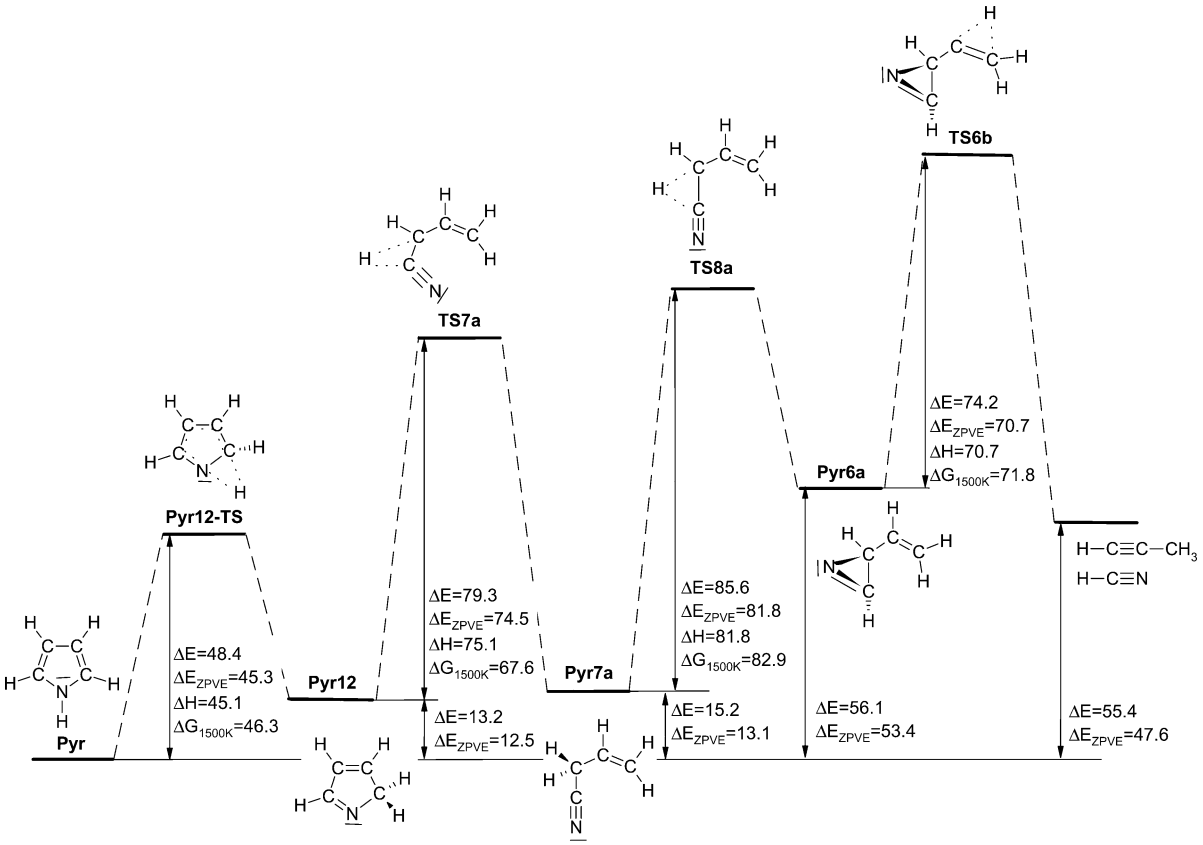

rather close to that of a triple bond; the C_k-C_{k+1} ($2 \le k \le 4$) bonds with the lengths of 1.449, 1.422, and 1.362 Å show an increase of double bond character as k increases. The bond length between the out-of-plane hydrogen and C_2 of 1.161 Å is elongated compared with the remaining H−C bonds, all equal of ≈1.085 Å. The TS7a structure is represented by a Lewis structure with a triple C−N bond and a single double C−C bond where the out-of-plane hydrogen moves away from C_2

TABLE 7: B3LYP/A Energy, Enthalpy (in Hartree), ZPVE (in kcal/mol), and Entropy (in cal/mol T) of the Structures in Charts 5−8[a]

structure	energy + 209	ZPVE	enthalpy + 209	entropy
Pyr	−1.17780	51.8	−1.09128	65.9
Pyr12-TS	−1.10060	48.6	−1.01942	65.1
Pyr12	−1.15682	51.1	−1.07135	66.1
TS5	−0.96675	42.5	−0.89241	77.6
TS6a	−1.03750	47.7	−0.95678	69.5
Pyr6a	−1.08835	49.0	−1.00498	72.1
TS6b	−0.97016	45.6	−0.89235	71.4
TS7a	−1.03039	46.3	−0.95164	71.1
Pyr7a	−1.15361	49.8	−1.06893	72.9
TS7b	−1.03512	46.3	−0.95598	72.9
Pyr7b	−1.04752	47.1	−0.96638	75.6
TS7c	−0.97245	44.2	−0.89610	75.4
TS8a	−1.01723	46.0	−0.93866	72.1
Pyr8a	−1.08835	49.0	−1.00498	72.1
TS8b	−0.97016	45.6	−0.89235	71.4

[a] The products HCN and CH_3CCH are characterized, respectively, by energies of −93.42845 and −116.66107 hartrees, ZPVE of 9.1 and 34.9 kcal/mol, enthalpies of −93.41112 and −116.60142 hartrees, and entropies of 40.7 and 61.3 cal/mol T.

toward C_3. Two possible pathways are found in the present work as starting from the intermediate Pyr7a: one of them passes through the azirine based intermediate Pyr6a. The other involves two hydrogen migrations, starting by the 4,5 H-migration and forming a carbene intermediate and ending by the 2,3 H one initiating the dissociation to HCN and propyne. As demonstrated in Charts 5−8, all of these stages have activation barriers (except TS8a) below the experimental value.

6. Summary

Two different facets of the N−H bond breaking in pyrrole have been thoroughly studied in the present work. One of them is related to the replacement of the hydrogen in the N−H bond by the alkali metal atoms, Li, Na, or K, giving rise to the formation of alkali metal pyrrolides. What we have demonstrated is the existence of a remarkable difference between Li-pyrrolide, on one hand, and the Na and K ones, on the other; although the former exists in two stable conformers, σ and π with the significant preference to the π one at least in the gas phase, the two latter only establish the stable π structure. A key factor of its stabilization is actually the formation of the $M^{+\delta}-N^{-\sigma}$ ionic pair (M = Li, Na, and K) which partly bares the metal atom so it likely behaves as a cation interacting with the pyrrole ring via a typical π−cation interaction and therefore, relative to the ionic asymptote $X^+ + Pyr^-$ (X = Li, Na, and K), shows the expected electrostatic trend, viz., K < Na < Li (cf. ref 16). Interestingly, relative to the neutral one, comprising of the infinitely separated X + Pyr$^\bullet$ (*X* = Li, Na, and K), the aforementioned trend changes to Na < K < Li which likely mirrors a larger polarizability of K compared to Na. Altogether, these features definitely imply a difference in behavior of Na and K, compared to Li, in biological systems.

Another facet is the "walk" of the hydrogen atom after the N−H bond breaking. Analyzing its possible "walks" along the ring, we have revealed four novel pathways of the pyrolysis of pyrrole, exiting with HCN and propyne. Together with the pathways proposed in refs 6c and 13e, the present ones may therefore be considered as possible pathways too. We believe that a firm answer on which one(s) of all of them is (are) dominant is left for experiment.

Acknowledgment. One of the authors, K.R.F.S., gratefully thanks the Flemish Institute for the Promotion of Science-Technology in Industry (IWT) for a grant. E.S.K. and A.C. acknowledge the Scientific Research Council of the University of Leuven for financial support. E.S.K. also thanks the Limburgs Universitair Centrum for a partial support within the "Bijzonder Onderzoeksfonds" (BOF). We also thank the referee for useful comments and valuable suggestions.

References and Notes

(1) (a) Hacker, R.; Kaufmann, E.; Schleyer, P. v. R.; Mahdi, W.; Dietrich, H. *Chem. Ber.* **1987**, *120*, 1533. (b) Johnson, T. J.; Alvey, L. J.; Brady, M.; Mayne, C. L.; Arif, A. M.; Gladysz, J. A. *Eur. J. Chem. A* **1995**, *1*, 294. (c) Frenzel, A.; Herbstirmer, R.; Klingebiel, U.; Noltemeyer, M.; Schafer, M. *Z. Naturforsch. B* **1995**, *50*, 1658. (d) Frenzel, A.; Gluth, M.; Herbstirmer, R.; Klingebiel, U. *J. Organomet. Chem.* **1996**, *514*, 281. (e) Drevs, H.; Schmeisser, A.; Hartung, H.; Baumeister, U. *Chem. Ber.* **1996**, *129*, 853. (f) Frenzel, A.; Herbstirmer, R.; Klingebiel, U.; Rudolph, S. *J. Organomet. Chem.* **1996**, *524*, 203. (g) Bertran, J.; Vinas, C.; Gomez, S.; Lamrani, M.; Teixidor, F.; Sillanpaa, R.; Kivekas, R. *Collect. Czech. Chem. Commun.* **1997**, *62*, 1263 and references therein.

(2) Goldfuss, B.; Schleyer, P. v. R.; Hampel, F. *Organomet.* **1997**, *16*, 5032.

(3) Lippard, S.; Berg, J. M. *Principles of Bioorganic Chemistry*; University Science Books: Mill Valley, CA, 1994.

(4) (a) Guo, B. C.; Conklin, B. J.; Castleman, A. W. *J. Am. Chem. Soc.* **1989**, *111*, 6506. (b) Klassen, J. S.; Anderson, S. G.; Blades, A. T.; Kebarle, P. *J. Phys. Chem.* **1996**, *100*, 14218. (c) More, M. B.; Ray, D.; Armentrout, P. B. *J. Phys. Chem. A* **1997**, *101*, 831. (d) Ma, J. C.; Dougherty, D. A. *Chem. Rev.* **1997**, *97*, 1303. (e) Hoyau, S.; Norrman, K.; McMahon, T. B.; Ohanessian, G. *J. Am. Chem. Soc.* **1999**, *121*, 8864. (f) Tsuzuki, S.; Yoshida, M.; Uchimaru, T.; Mikami, M. *J. Phys. Chem. A* **2001**, *105*, 769 and references therein.

(5) Frisch, M. J.; Trucks, G. W.; Schlegel, H. B.; Scuseria, G. E.; Robb, M. A.; Cheeseman, J. R.; Zakrzewski, V. G.; Montgomery, J. A., Jr.; Stratmann, R. E.; Burant, J. C.; Dapprich, S.; Millam, J. M.; Daniels, A. D.; Kudin, K. N.; Strain, M. C.; Farkas, O.; Tomasi, J.; Barone, V.; Cossi, M.; Cammi, R.; Mennucci, B.; Pomelli, C.; Adamo, C.; Clifford, S.; Ochterski, J.; Petersson, G. A.; Ayala, P. Y.; Cui, Q.; Morokuma, K.; Malick, D. K.; Rabuck, A. D.; Raghavachari, K.; Foresman, J. B.; Cioslowski, J.; Ortiz, J. V.; Stefanov, B. B.; Liu, G.; Liashenko, A.; Piskorz, P.; Komaromi, I.; Gomperts, R.; Martin, R. L.; Fox, D. J.; Keith, T.; Al-Laham, M. A.; Peng, C. Y.; Nanayakkara, A.; Gonzalez, C.; Challacombe, M.; Gill, P. M. W.; Johnson, B. G.; Chen, W.; Wong, M. W.; Andres, J. L.; Head-Gordon, M.; Replogle, E. S.; Pople, J. A. *Gaussian 98*, revision A.5; Gaussian, Inc.: Pittsburgh, PA, 1998.

(6) (a) Martin, J. M. L.; El-Yazal, J.; Francois, J.-P. *Mol. Phys.* **1995**, *86*, 1437. (b) Simandiras, E. D.; Handy, N. C.; Amos, R. D. *J. Phys. Chem.* **1988**, *92*, 1739. (c) Bacskay, G. B.; Martoprawiro, M.; Mackie, J. C. *Chem. Phys. Lett.* **1999**, *300*, 321. (d) See also: Jursic, B. S. *J. Mol. Struct. (THEOCHEM)* **1998**, *454*, 277. (e) For earlier publications on pyrrole, see: Kao, J.; Hinde, A. L.; Radom, L. *Nouv. J. Chim.* **1979**, *3*, 473 and references therein.

(7) (a) Nygaard, L.; Nielsen, J. T.; Kirchheiner, J.; Maltesen, G.; Rastrup-Andersen, J.; Sørensen, G. O. *J. Mol. Struct.* **1969**, *3*, 491. (b) Harmony, M. D.; Lawrie, V. W.; Kuczowski, R. L.; Schwendeman, R. H.; Ramsey, R. D.; Lovas, F. J.; Lafferty, W. J.; Maki, A. G. *J. Phys. Chem. Ref. Data* **1979**, *8*, 619. (c) See also the recent work: Geidel, E.; Billes, F. *J. Mol. Struct. (THEOCHEM)* **2000**, *507*, 75 and references therein.

(8) Rienstra-Kiracofe, J. C.; Graham, D. E.; Schaefer, H. F., III. *Mol. Phys.* **1998**, *94*, 767.

(9) Navarro, R.; Orza, J. M. *Ann. Quim.* **1983**, *Ser. A 79*, 557, 571; **1984**, *Ser. A 80*, 59; **1985**, *Ser. A 81*, 5.

(10) Roos, B. O.; Malmqvist, P.-Å.; Molina, V.; Serrano-Andrés, L.; Merchán, M. *J. Chem. Phys.* **2002**, *116*, 7526.

(11) Bacskay, G. B.; Martoprawiro, M.; Mackie, J. C. *Chem. Phys. Lett.* **1998**, *290*, 391.

(12) (a) Lifshitz, A.; Tamburu, C.; Suslensky, A. *J. Phys. Chem.* **1989**, *93*, 5802. (b) Mackie, J. C.; Colket, M. B.; Nelson, P. F.; Esler, M. *Int. J. Chem. Kinet.* **1991**, *23*, 733. (c) Doughty, A.; Mackie, J. C. *J. Phys. Chem.* **1992**, *96*, 272. (d) Dubnikova, F.; Lifshitz, A. *J. Phys. Chem. A* **1998**, *102*, 10880. (e) Martoprawiro, M.; Bacskay, G. B.; Mackie, J. C. *J. Phys. Chem. A* **1999**, *103*, 3923. See also references therein.

(13) The G2-(MP2) calculations, performed in ref 12e, are based on CASSCF/cc-pVDZ geometries and frequencies scaled by a factor of 0.92 (see p 3924 of ref 12e for computational details).

(14) (a) Sunderlin, L. S.; Panu, D.; Puranik, D. B.; Ashe, A. J., III.; Squires, R. R. *Organometallics* **1994**, *13*, 4732. (b) Bachrach, S. M. *J. Org. Chem.* **1993**, *58*, 5414.

(15) Doughty, A.; Bacskay, G. B.; Mackie, J. C. *J. Phys. Chem.* **1994**, *98*, 13546.

(16) Meyer, E. A.; Castellano, R. K.; Diederich, F. *Angew. Chem., Int. Ed.* **2003**, *42*, 1210 and references therein.